

Article

The Study of Phase Transformation Behaviors for 38MnB5Nb Ultra High-Strength Steel by CCT Curves and TTT Curves

Ping Luo ^{1,*}, Xianjun Li ¹, Wenliang Zhang ¹, Xiao Liang ² , Zhunli Tan ^{3,*}, Decheng Wang ¹, Chao Jiang ¹, Junqing Hou ¹ and Lizhuang Sun ¹

¹ Beijing Research Institute of Mechanical and Electrical Technology Ltd., Beijing 100083, China

² The College of Mechanical and Electrical Engineering, Nanjing University of Aeronautics and Astronautics, Nanjing 210016, China

³ Material Science & Engineering Research Center, School of Mechanical, Electronic and Control Engineering, Beijing Jiaotong University, Beijing 100044, China

* Correspondence: 18811795072@163.com (P.L.); tzli@bjtu.edu.cn (Z.T.)

Abstract: To elucidate the phase transformation behaviors for 38MnB5Nb ultra high-strength steel, the continuous cooling transformation (CCT) and time-temperature-transformation (TTT) curves were determined by the thermal expansion method with different cooling rates and isothermal temperatures after complete austenitization. To be more accurate, the microstructure was observed and the hardness was tested. The results showed that the starting and ending transformation temperatures of austenite during heating are 748 °C and 805 °C, respectively. Bainite's start temperature is between 540 °C and 550 °C, while martensite's start temperature is about 310 °C. The critical cooling transformation rate is between 10 °C/s and 15 °C/s. The results showed that the microstructures are severely related to the cooling rate during the continuous cooling process and are related to isothermal temperatures during the isothermal process. The relationship between hardness and the microstructure was investigated and hardness is severely related to the microstructure. Based on the results of CCT curves compared with the conventional 22MnB5 hot stamping steel, the studied 38MnB5Nb steel is more beneficial for selective cooling processes.

Keywords: ultra high-strength steel; CCT curves; TTT curves; microstructure; hardness



Citation: Luo, P.; Li, X.; Zhang, W.; Liang, X.; Tan, Z.; Wang, D.; Jiang, C.; Hou, J.; Sun, L. The Study of Phase Transformation Behaviors for 38MnB5Nb Ultra High-Strength Steel by CCT Curves and TTT Curves. *Metals* **2023**, *13*, 190. <https://doi.org/10.3390/met13020190>

Academic Editors: Dongsheng Qian, Feng Wang and Carlos Garcia-Mateo

Received: 22 December 2022

Revised: 10 January 2023

Accepted: 16 January 2023

Published: 18 January 2023



Copyright: © 2023 by the authors. Licensee MDPI, Basel, Switzerland. This article is an open access article distributed under the terms and conditions of the Creative Commons Attribution (CC BY) license (<https://creativecommons.org/licenses/by/4.0/>).

1. Introduction

It is well-known that the problems in energy production and environmental protection have been becoming severe. According to statistics, the global oil reserves can only cover 40 years with the current extraction rate of oil [1–3]. Owing to the consumption of relatively high oil resources for the production of car fuel and the environmental pollution of car emissions, the automotive industry is still facing growing pressure to reduce the weight of vehicles and improve crash performance since approximately 75% of the fuel consumption is severely related to the car weight [4]. In order to reduce the vehicle weight and improve crash safety performances, ultra high-strength steels (UHSS) have been applied to manufacture vehicle components, such as A-pillars, B-pillars, roof rails, and so on. In this context, hot stamping steels have been investigated and used [5,6].

Generally, the common hot stamping steel is 22MnB5, which has been widely used to manufacture A-pillars, B-pillars, and so on, successfully. Gazi University in Turkey investigated the effect of heat treatment conditions on microstructural features and mechanical properties of 22MnB5 hot stamping steel [7]. Finally, the optimized heat treatment process parameters were suggested to make A-pillars and B-pillars. 22MnB5 ultra high-strength steel was applied to manufacture bumpers and pillars by the technology of hot stamping and so the thickness of the parts was reduced owing to the good performance with a final strength above 1500 MPa [8,9]. Tingzhi Si et al. studied the effects of microalloying with Ti + Nb + V on the hydrogen permeation and damage behaviors of the 22MnB5 hot

stamping steel [10]. Their research implied that the addition of Ti + Nb + V for 22MnB5 steel would largely reduce the hydrogen diffusion coefficient, which is of great importance for A-pillars and B-pillars made of ultra high-strength steel. Finally, a model was proposed to illustrate the improvements in hydrogen diffusion and hydrogen damage in the hot stamping steel.

At the same time, other technologies were applied to increase the strength of parts so as to reduce their weights. Hossein Nassiraei et al. [11] proposed an FE model to investigate the effect of the collar plate size and joint geometry on the static strength of X-joints at elevated temperatures. Finally, a new equation was proposed for determining the ultimate strength of X-joints reinforced with collar plates subjected to compressive load at elevated temperatures, which is a good means of lightweight. At the same time, Erfan Maleki [12–15] suggested shot peening processes to increase the tensile strength and fatigue strength and so on of parts, so the thickness of parts can be reduced and the weights are also reduced at the same time.

Recently, novel hot stamping methods have been developed to obtain a part made of 22MnB5 steel consisting of both a high energy-absorption region and a high intrusion-resistance region through a single process [16,17]. To achieve the above goal, innovative processing strategies such as selective heating, selective cooling, and tailored tooling were used to tailor the material mechanical properties [18–20]. The hot stamping by partition heating to produce 22MnB5 steel B-pillars was investigated to tailor parts with average tensile strengths of 1565 MPa and 626 MPa in the high- and low-temperature regions, respectively [21].

With the further demand for lightweight vehicle parts, 38MnB5Nb ultra high-strength steel was developed. The tensile strength can reach as high as 2000 MPa with the treatment of hot stamping or quenching. Guo et al. studied the effects of 0.054 Nb on the microstructure and mechanical properties of 38MnB5 steel [22]. The results indicated that the addition of appropriate Nb can refine microstructures and enhance properties including tensile strength, yield strength, and elongation. Our previous work studied the high-temperature flow behavior of 38MnB5Nb steel taking into consideration the deformation temperature, strain rate, and type of microstructure [23]. Finally, hot-formed U-shaped parts were investigated by means of numerical and experimental analysis. However, the microstructure evolution behavior is not studied yet.

The phase transformation evolution behavior of steel is critical for manufacturing qualified components. For example, the phase transformation behavior of steel can be used to guide the design and optimize the hot stamping process, as well as the design of hot stamping mold, and so on. So, in this paper, the continuous cooling transformation (CCT) curves and time-temperature-transformation (TTT) curves of 38MnB5Nb ultra high-strength steel were determined by the thermal expansion method with different cooling rates and isothermal temperatures after complete austenization.

2. Methods

The chemical compositions of the studied 38MnB5Nb steel plates that were manufactured with the process of hot-rolling by ShouGang in China are presented in Table 1. For comparison, the chemical compositions of the conventional 22MnB5 hot stamping steel are also listed in Table 1. It can be seen that both of them are added with amounts of Mn, which can enhance the hardenability of the steel. So, it can be manufactured with the hot stamping processes. Meanwhile, compared with 22MnB5 steel [24], the C content is increased by about 0.11 and the Nb is added by about 0.05 in weight percentage, respectively. According to the research [25], both the increment of C and the addition of Nb are beneficial for the improvement of hardenability and the enhancement of strength after the hot stamping processes, which make a contribution to the lightweight of components. The initial microstructures consist of ferrite and pearlite, as shown in Figure 1a, and the white areas stand for ferrite with a grain size of 16 μm , while the black areas are pearlite with a grain size of 8~15 μm . It should be noted that before dilatometric experiments, the 38MnB5Nb

steel plates were homogenized. They were heated to 950 °C and held for 30 min, followed by cooling to room temperature inside the furnace (Beijing Research Institute of Mechanical and Electrical Technology Ltd., Beijing, China).

Table 1. Compositions of the 38MnB5Nb and 22MnB5 steel (weight percentage, wt%).

Steel	C	Si	Mn	Cr	B	Nb	Fe
38MnB5Nb	0.36	0.24	1.39	0.19	0.005	0.05	Bal.
22MnB5	0.25	0.24	1.36	0.2	0.005	~	Bal.

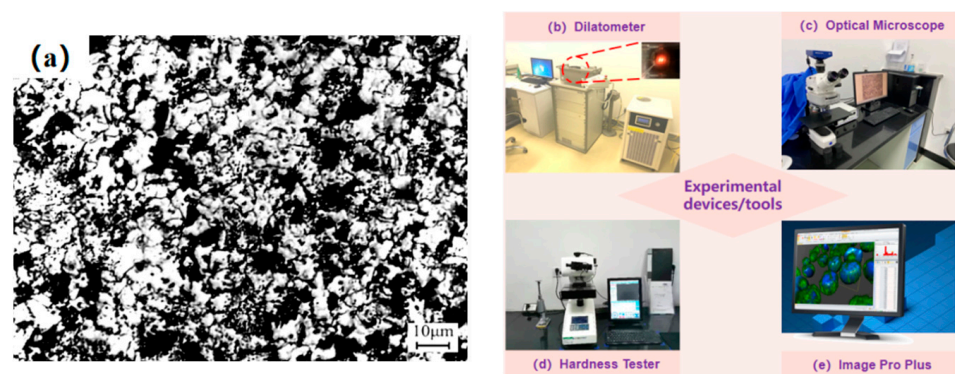


Figure 1. Initial microstructures of 38MnB5Nb and experimental devices/tools. (a) Initial microstructures; white areas stand for ferrite and black areas stand for pearlite, (b) dilatometer, (c) optical microscope, (d) hardness tester, and (e) Image Pro Plus.

A dilatometer (Bähr D805 L, Bachmuseum, Germany) equipped with quartz push-rods (Figure 1b) was used to determine the phase transformation temperatures and phase transformation time systematically with specimens 10 mm in length, 4 mm in width, and 2 mm in thickness, as shown in Figure 2a. A tangent method was used to determine the phase transformation temperatures under different cooling rates and phase transformation time under different isothermal temperatures.

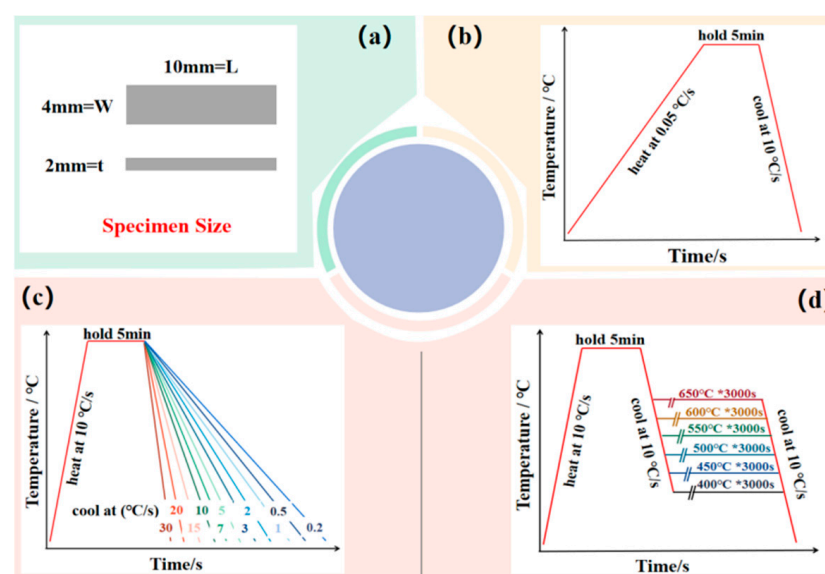


Figure 2. Size of the specimen and schematic graphs of different dilatometric experiments. (a) Specimens' size, (b) Ac1 and Ac3 dilatometric experiments, (c) CCT dilatometric experiments, and (d) TTT dilatometric experiments.

The dilatometric experiment for Ac1 and Ac3 is as follows. Firstly, the phase transformation temperatures (Ac1: 748 °C and Ac3: 805 °C) were measured as shown in Figure 3 [26]. During this experiment, the specimen was slowly heated to 920 °C at 0.05 °C/s. After holding for 5 min at 920 °C, it was quenched to room temperature at 50 °C/s, as shown in Figure 2b.

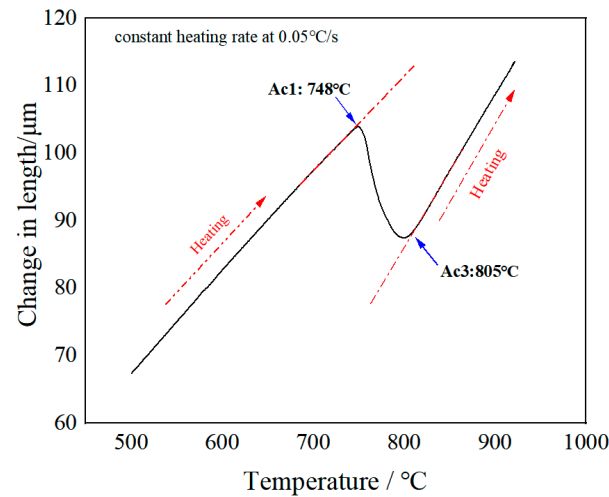


Figure 3. The phase transition temperature of 38MnB5Nb steel measured by the thermal expansion method. Ac1, austenite's start transformation temperature and Ac3, austenite's start transformation temperature.

The dilatometric experiments for CCT curves is as follows. Secondly, the specimens were heated to 920 °C with a constant heating rate of 10 °C/s and cooled to an ambient temperature of about 30 °C with different constant cooling rates of 0.2 °C/s, 0.5 °C/s, 1 °C/s, 2 °C/s, 3 °C/s, 5 °C/s, 7 °C/s, 10 °C/s, 15 °C/s, 20 °C/s, and 30 °C/s after holding for 5 min at 920 °C, as shown in Figure 2c.

The dilatometric experiments for TTT curves is as follows. Thirdly, the specimens were heated to 920 °C with a constant heating rate of 10 °C/s; then, they were fast-cooled with a cooling rate of 10 °C/s (the selection of the cooling rate is based on the CCT curves). It can be seen that no transformation can happen during the cooling stage from 920 °C to the different isothermal temperatures with a cooling rate of 10 °C/s to the isothermal temperatures of 400 °C, 450 °C, 500 °C, 550 °C, 600 °C, and 650 °C and hold for 3000 s at the above isothermal temperature. Finally, the specimens were fast-cooled to 30 °C with a cooling rate of 30 °C/s, as shown in Figure 2d.

Microstructural analysis and hardness tests were carried out by optical microscope (OM, Zeiss, Oberkochen, Germany, Figure 1c) after mechanical carefully polishing and etching in 2% nital solution for about 10 s. The hardness of the specimens for the CCT dilatometric experiments were tested with a Vickers hardness tester (Beijing Times, Beijing, China, Figure 1d). During hardness testing, the load was kept at about 10 gf and the time was kept for 10 s. Five values were measured for all CCT curve specimens and the average values were adopted. Meanwhile, Image Pro Plus software (Figure 1e) was applied to distinguish and characterize microstructures.

3. Results and Discussion

3.1. CCT Curves

The relationship curves between length changes of dilatometry specimens and temperatures during the cooling of dilatometric experiments for CCT curves are shown in Figure 4(a-1-k-1). The microstructures of different cooling rates are shown in Figure 4(a-2-k-2). The corresponding images treated by Image Pro Plus software are displayed on the right of the microstructures (marked by Figure 4(a-3-k-3)). Meanwhile, the phase transformation temperatures during the cooling stage with different constant cooling rates are summarized in Table 2. It

displayed that the phase start transformation temperatures and phase finish transformation temperatures are severely relative to the cooling rate, which means the different phase start transformation temperatures and phase finish transformation temperatures are reaped under different constant cooling rates. It showed that the start transforming temperatures under all cooling rates between $0.2\text{ }^{\circ}\text{C/s}$ and $30\text{ }^{\circ}\text{C/s}$ are below A_{c1} . It can be seen that the phase start transformation temperatures and phase finish transformation temperatures are relatively high when cooling rates are between $0.2\text{ }^{\circ}\text{C/s}$ and $3\text{ }^{\circ}\text{C/s}$, and the transforming temperatures are decreased as the cooling rates increased. It can be inferred that ferrite and pearlite with a grain size of about $40\text{--}60\text{ }\mu\text{m}$ are obtained for those cooling rates, which is consistent with the microstructures (shown in Figure 4(a-2-e-2)). Figure 4(a-3-e-3) show that the fraction of ferrite is decreased while the fraction of pearlite is increased with the increment of cooling rate from $0.2\text{ }^{\circ}\text{C/s}$ and $3\text{ }^{\circ}\text{C/s}$. At the same time, there exists obvious inflection points between start and finish transformation temperatures with the cooling rates of $0.2\text{ }^{\circ}\text{C/s}$ and $0.5\text{ }^{\circ}\text{C/s}$, which can be explained by the phase transformation changing from ferrite to pearlite. Compared with the cooling rates of $0.2\text{ }^{\circ}\text{C/s}$ and $3\text{ }^{\circ}\text{C/s}$, when the cooling rate reached $5\text{ }^{\circ}\text{C/s}$, despite the first transformation temperatures being relatively high, the finish transformation temperature is reduced to $540\text{ }^{\circ}\text{C}$. According to the microstructure as shown in Figure 4(f-2), austenite is firstly transformed to ferrite and pearlite, and then the little untransformed austenite is transformed to bainite during cooling at $5\text{ }^{\circ}\text{C/s}$. However, the first transformation temperature is about $320\text{ }^{\circ}\text{C}$ with cooling rates at $7\text{ }^{\circ}\text{C/s}$ and $10\text{ }^{\circ}\text{C/s}$, which is largely lower than that of cooling at $5\text{ }^{\circ}\text{C/s}$. This is owing to the absence of the ferrite and pearlite transformation; as a result, bainite and martensite are obtained (shown in Figure 4(g-2-h-2)). Meanwhile, only martensite is formed with cooling rates at $15\text{ }^{\circ}\text{C/s}$ to $30\text{ }^{\circ}\text{C/s}$. So, martensite's start temperature is about $310\text{ }^{\circ}\text{C}$, and it is obvious that the critical cooling rate is between $10\text{ }^{\circ}\text{C/s}$ and $15\text{ }^{\circ}\text{C/s}$.

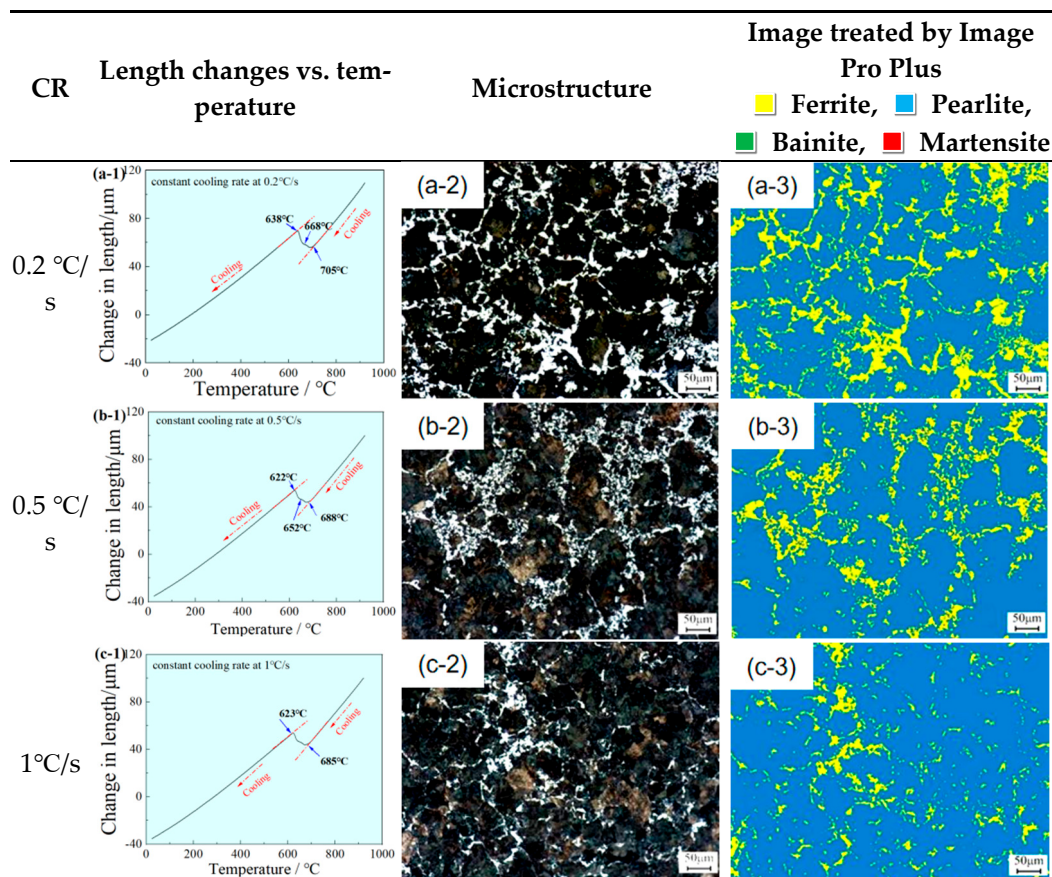


Figure 4. Cont.

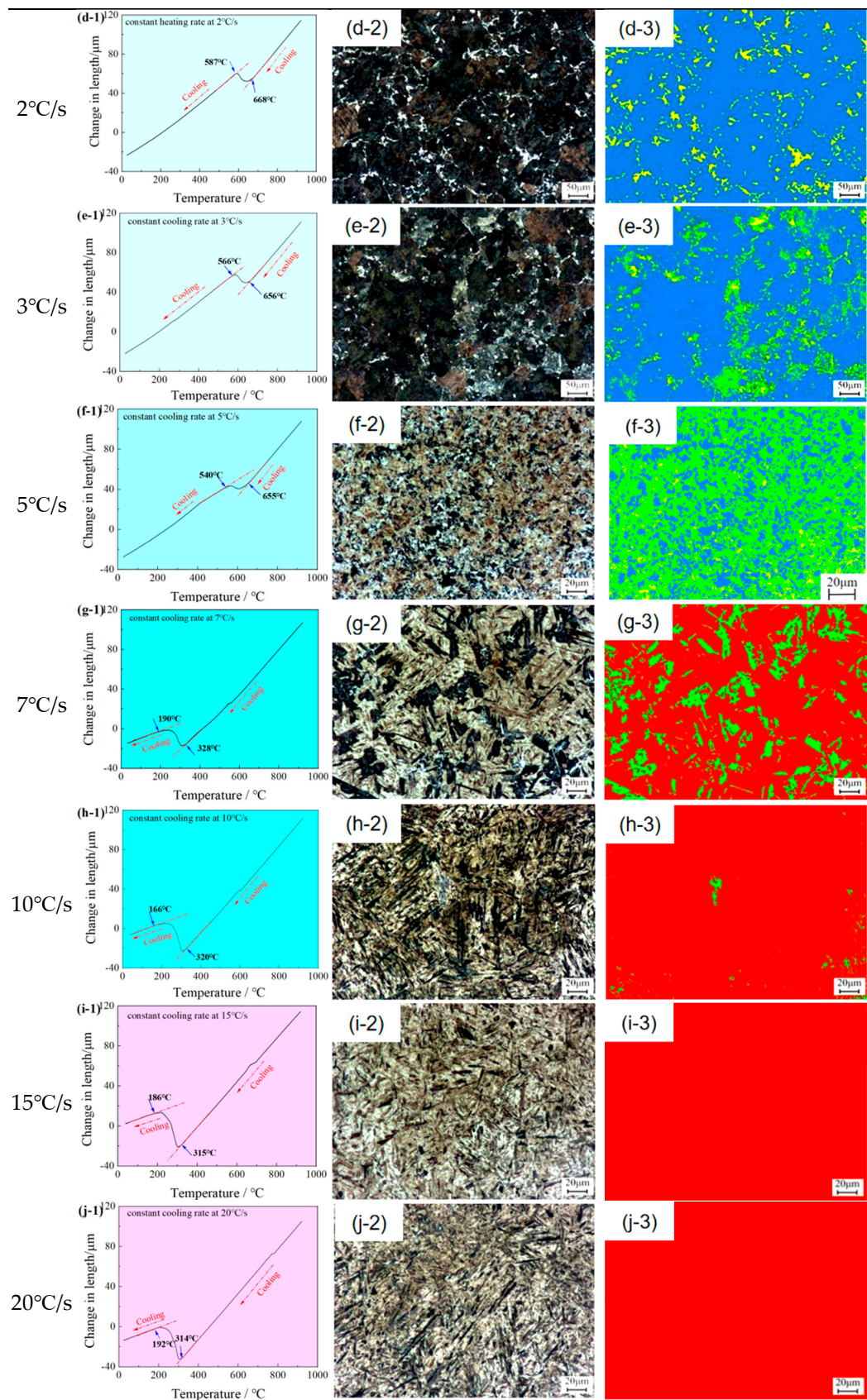


Figure 4. Cont.

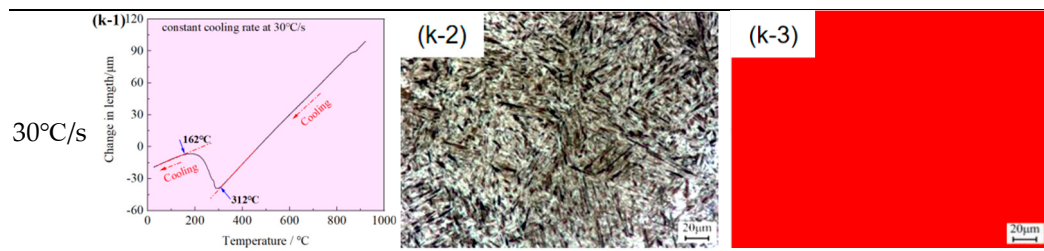


Figure 4. The relationship curves between length changes and temperature for CCT curve experiments (a-1–k-1); the microstructures of different cooling rates (a-2–k-2); the images of different cooling rates (a-3–k-3).

Table 2. Transformation temperatures under different cooling rates of 38MnB5Nb steel.

CR, °C/s	First Transformation Temperature, °C	Second Transformation Temperature, °C	Third Transformation Temperature, °C
0.2	705	668	638
0.5	688	652	622
1	685	623	-
2	668	587	-
3	656	566	-
5	655	540	-
7	328	190	-
10	320	166	-
15	315	186	-
20	314	192	-
30	312	162	-

The Vickers hardness (HV) of each specimen were measured after dilatometric experiments for CCT curves, and the results are presented in Figure 5. Hardness is increased slightly (221 HV → 224 HV), with cooling rates between 0.2 °C/s and 2 °C/s. It is consistent with the microstructure analysis that ferrite and pearlite, whose hardnesses are generally low are formed within the above cooling rates. However, hardness is obviously increased (285 HV → 497 HV), as the cooling rates ranges from 3 °C/s to 7 °C/s. This is principally because in this cooling rate range, austenite is transformed to ferrite, pearlite, bainite, and martensite, and the fraction of bainite and martensite increased while ferrite disappeared as the cooling rates increased. Generally, for the steel with the same chemical compositions, the hardness of ferrite and pearlite is lowest, and then the bainite; while martensite has the highest hardness. Meanwhile, with the cooling rate raised from 10 °C/s to 15 °C/s, hardness is improved relatively slightly (557 HV → 576 HV). This can be owing to the fact that austenite has the same transformation of austenite to bainite and martensite multiphase. The types of microstructures which affect the hardness mostly are not changed. So, the hardness changes with little range. From the above analysis, it can be inferred that the hardness of specimens consisting of bainite is between 497 Hv and 557 HV. Finally, hardness is kept at the level of 580 HV. From the dilatometric and microstructural results, it can be seen that austenite is transformed to martensite as the cooling rates exceeded 15 °C/s; thus, hardness is almost not variable.

Based on the above analysis of the dilatometric results, microstructure results, and hardness results, the continuous cooling transformation (CCT) curves are plotted, as shown in Figure 6a. Additionally, the CCT curves of 22MnB5 hot stamping steel are also shown in Figure 6b [27]. Obviously, compared with 22MnB5 hot stamping steel, the ferrite/pearlite and bainite transformations of 38MnB5Nb steel are shifted to the right, which illustrates that the hardenability of 38MnB5Nb steel is higher than that of 22MnB5 steel and it is more easy to obtain the desired martensite microstructure during the hot stamping processes. Martensite's start transformation temperature was reduced from above 400 °C/s to about 310 °C/s; as a result, martensite's finish transformation was reduced. The

critical cooling rate is reduced from 30 °C/s to slightly above 10 °C/s but below 15 °C/s, which is of great significance to the hot stamping process, particularly the quenching process. The phase transformation temperature of Ac3 was largely decreased from 880 °C to 805 °C, which means that the temperature for austenitization during hot stamping processes can be decreased to 850 °C–880 °C, while the phase transformation temperature of Ac1 had little change. Importantly, it can be seen that there exists a wide cooling rate range (0.2 °C/s~3 °C/s) to obtain the ferrite and pearlite microstructure without any bainite and/or martensite for 38MnB4Nb steel, while it is more easily transformed to the ferrite, pearlite, and bainite microstructure for 22MnB5 steel. This characteristic is beneficial for selective cooling to tailor the material mechanical properties so as to meet the requirements that the upper region consisted of martensitic microstructure for high intrusion resistance while the lower region consisted of softer phases (ferrite and pearlite) to provide high-energy absorption capacity to improve side crash performance, which is helpful to A-pillars and B-pillars [13]. It is widely known that developing a part consisting of both a high energy-absorption region and a high intrusion-resistance region is the future trend [14,15].

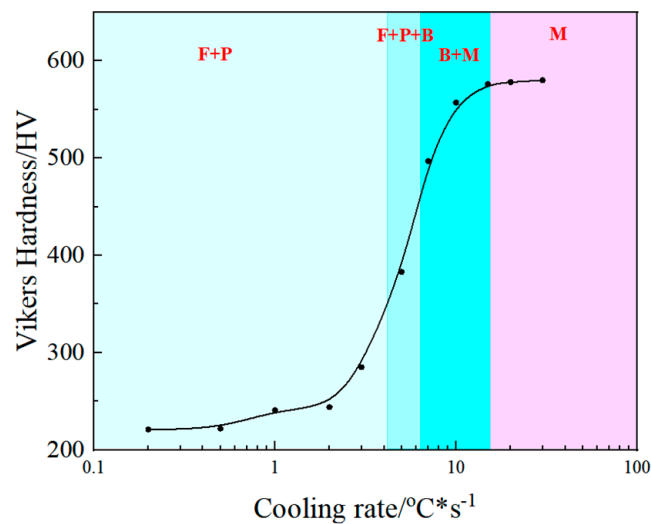


Figure 5. Relationship between hardness and cooling rates of the studied steel.

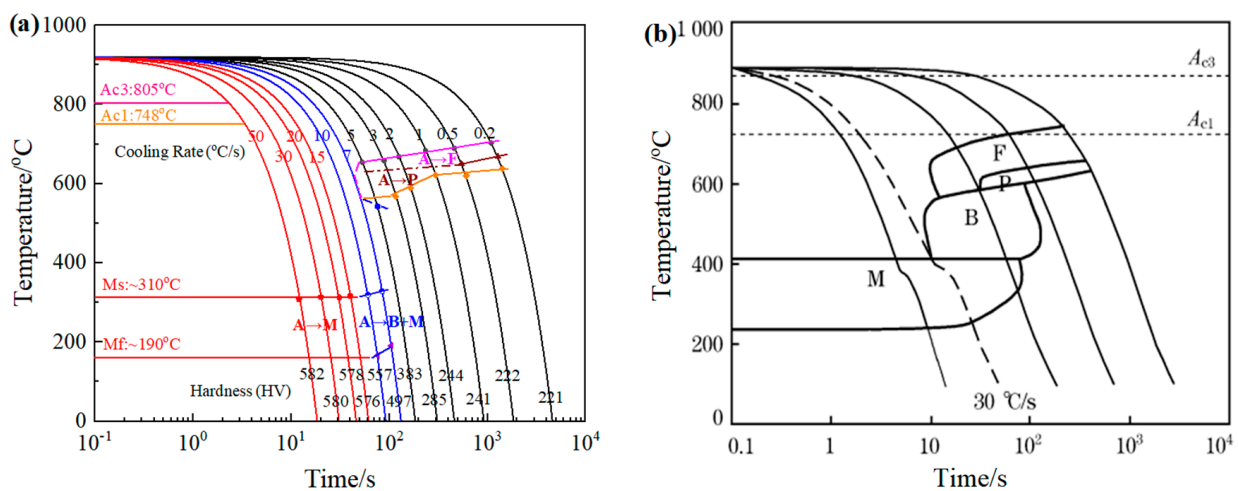


Figure 6. CCT curves of 38MnB5Nb steel (a) and 22MnB5 steel; (b) data from [27]. A, austenite; F, ferrite; P, pearlite; B, bainite; M, martensite.

3.2. TTT Curves

The relationship curves between length changes of dilatometry specimens and temperatures during cooling and the isothermal stage of the dilatometric experiments for TTT curves are shown in Figure 7(a-1–f-1). These curves show that there is no transformation during the subsequent cooling after isothermal treatment at different temperatures. Combining with the relationship curves between the length changes of dilatometry specimens and time during the isothermal stage of the dilatometric experiments for TTT curves, as well as the microstructure, it can be inferred the austenite is completely transformed to ferrite/pearlite or bainite during isothermal treatment at different temperatures for 3000 s. The relationship curves between the length changes of dilatometry specimens and time during the isothermal stage of the dilatometric experiments for TTT curves are displayed in Figure 7(a-2–f-2). At the same time, the start time and finish times at different temperatures are summarized in Table 3. It is obvious that the start time, as well as finish time, are different with the different isothermal temperatures and that the transformation time is within 350 s for the isothermal transformation. Generally, the start time and finish time are different owing to the fact that the transformation-driven force and the diffusion coefficient of carbon atoms are different at different isothermal temperatures. The shortest start time is an isothermal temperature of 650 °C and the longest start time is an isothermal temperature of 400 °C. Meanwhile, the shortest finish time is 650 °C and the longest finish time is 400 °C. The microstructures of all the specimens for TTT curves are shown in Figure 7(a-3–f-3). Obviously, it consists of ferrite and pearlite when isothermal at 650 °C, 600 °C, and 550 °C. However, bainite is obtained when isothermal at 500 °C, 450 °C, and 400 °C. So, it can be deduced that bainite's start temperature is between 500 °C and 550 °C. However, from the above CCT curves analysis, the microstructure is ferrite, pearlite, and bainite with a cooling rate of 5 °C/s, in which the transformation start temperature is 655 °C and the transformation finish temperature is 540 °C (as shown in Figure 6a). The microstructure is ferrite and pearlite with a cooling rate of 3 °C/s, in which the transformation start temperature is 656 °C and the transformation finish temperature is 566 °C (as shown in Figure 6a). This means that bainite is formed at a temperature of about 540 °C but below 566 °C, which indicates that bainite's start temperature is between 540 °C and 566 °C. In summary, bainite's start temperature is between 540 °C and 550 °C from the CCT curve and TTT curve results. It is of great importance to determine the second heating temperature of the partition slow cooling tailored properties hot forming process (TPP-S) and partition fast cooling tailored properties hot forming process (TPP-F) [23].

Table 3. Transformation times under different isothermal temperatures of studied steel.

ISO-TEM/°C	Start Time/s	Finish Time/s	ISO-TEM/°C	Start Time/s	Finish Time/s
400	75	342	550	10	135
450	25	252	600	8	138
500	10	218	650	4	72

Finally, based on the above analysis, the time-temperature-transformation (TTT) curves are plotted, as shown in Figure 8, which is of great importance for designing the selective heating process and isothermal transformation parameters, such as temperature and time, and so on.

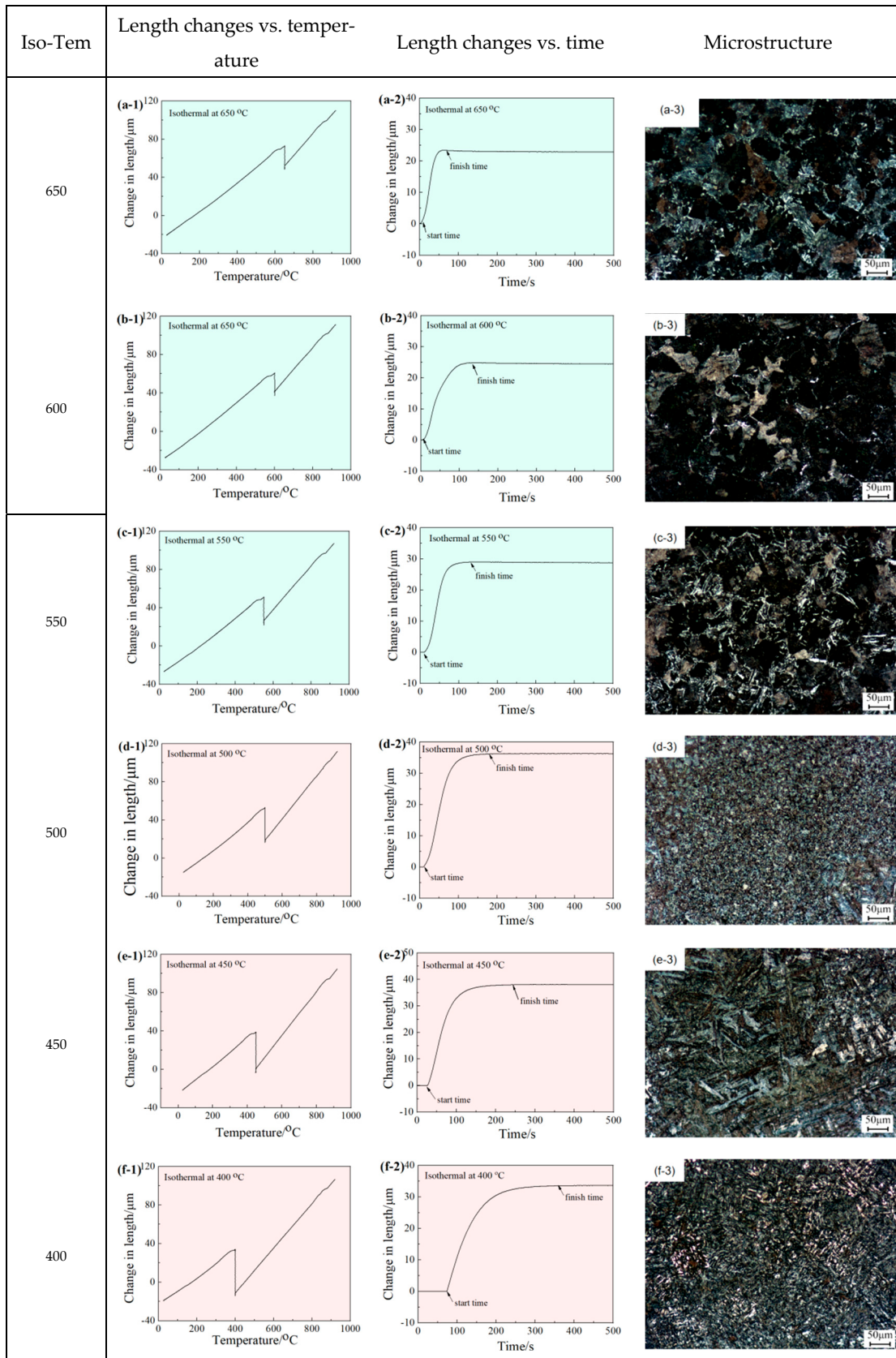


Figure 7. The relationship curves between length changes and temperature for TTT curve experiments (a-1–f-1); the relationship curves between length changes and time for TTT curve experiments during the isothermal stage (a-2–f-2); the microstructures of different isothermal temperature (a-3–f-3).

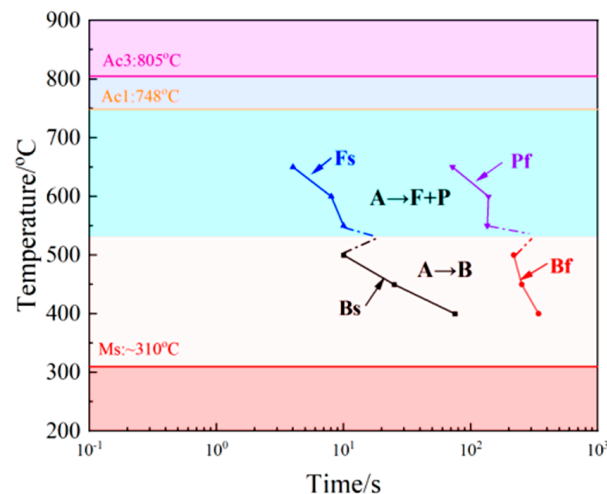


Figure 8. TTT curves of 38MnB5Nb steel. A, austenite; F, ferrite; P, pearlite; B, bainite; Fs, ferrite's start transformation line; Pf, pearlite's finish transformation line; Bs, bainite's start transformation line; Bf, bainite's finish transformation line.

4. Conclusions

The continuous cooling transformation (CCT) curves, as well as the time-temperature-transformation (TTT) curves, are obtained from the 38MnB5Nb steel. The phase transformation behaviors during continuous cooling and isothermal is investigated. The following conclusions are summarized.

The Ac1 and Ac3 are 748 °C and 805 °C. Combining the results of CCT curves and TTT curves, bainite's start temperature is between 540 °C and 550 °C; while martensite's start temperature is about 310 °C; the critical cooling rate is between 10 °C/s and 15 °C/s.

The microstructures are severely related to the cooling rate during the continuous cooling process. Ferrite and pearlite microstructure's are obtained with cooling rate ranging between 0.2 °C/s and 3 °C/s. Ferrite, pearlite, bainite, and martensite are reaped with cooling rate ranges of 3 °C/s to 7 °C/s; bainite and martensite are obtained with cooling rate ranges of 7 °C/s to 10 °C/s; only martensite is reaped with a cooling rate exceeding 15 °C/s.

The microstructures are related to isothermal temperatures during the isothermal process. It consists of ferrite and pearlite when the isothermal is at 650 °C, 600 °C, and 550 °C. However, bainite is obtained when the isothermal is at 500 °C, 450 °C, and 400 °C.

Hardness is severely related to cooling rates, as well as microstructures. The hardness of ferrite and pearlite is about 220 HV to 240 HV; the hardness of bainite is between 497 HV and 557 HV; while the hardness of martensite is as high as 580 HV.

Compared with the conventional hot stamping 22MnB5 steel, the studied 38MnB5Nb steel is more beneficial for selective cooling processes.

Author Contributions: Conceptualization, P.L.; data curation, X.L. (Xiao Liang), D.W., J.H. and L.S.; formal analysis, P.L.; funding acquisition, X.L. (Xianjun Li) and D.W.; investigation, P.L., Z.T. and L.S.; methodology, P.L., X.L. (Xianjun Li), W.Z., X.L. (Xiao Liang) and J.H.; project administration, W.Z. and C.J.; resources, C.J.; supervision, X.L. (Xianjun Li), W.Z. and C.J.; validation, Z.T.; visualization, L.S.; writing—original draft, P.L.; writing—review & editing, X.L. (Xianjun Li), X.L. (Xiao Liang), Z.T. and D.W. All authors have read and agreed to the published version of the manuscript.

Funding: This research was funded by National Science and Technology Major Project of China, grant number 2018ZX04023002, and National Science and Technology Major Project of China, grant number 2018ZX04044001.

Institutional Review Board Statement: Not applicable.

Informed Consent Statement: Not applicable.

Data Availability Statement: Not applicable.

Acknowledgments: The authors express thanks to the National Science and Technology Major Project of China, grant number 2018ZX04023002, and the National Science and Technology Major Project of China, grant number 2018ZX04044001.

Conflicts of Interest: The authors declare no conflict of interest.

Nomenclature

UHSS	ultra high-strength steel
CCT curves	continuous cooling transformation curves
OM	optical microscope
Iso-Tem	isothermal temperature
TPP-F	partition fast cooling tailored properties hot forming process
FE model	finite element model
TTT curves	time-temperature-transformation curves
CR	cooling rate
TPP-S	partition slow cooling tailored properties hot forming process

References

- Chen, J. Discussion of the modern electronic technology application and future development trend on automobile. *Appl. Mech. Mater.* **2012**, *155–156*, 627–631. [CrossRef]
- Merklein, M.; Johannes, M.; Lechner, M.; Kuppert, A. A review on tailored blanks—Production, applications and evaluation. *J. Mater. Process. Technol.* **2014**, *214*, 151–164. [CrossRef]
- Staeves, J.; Pfestorf, M. Einsatz höherfester Stähle im Automobilbau. In *Umformtechnisches Kolloquium Darmstadt*; Groche, P., Ed.; Darmstadt, Germany, 2003; pp. 51–61. Available online: https://www.staeves.de/veroeffentlichung/UKD_2003PPT.pdf (accessed on 1 December 2022).
- Li, Y.; Lin, Z.; Jiang, A.; Chen, G. Experimental study of glass-fiber mat thermoplastic material impact properties and lightweight automobile body analysis. *Mater. Des.* **2004**, *25*, 579–585. [CrossRef]
- Schwingschlogl, P.; Niederhofer, P.; Merklein, M. Investigation on basic friction and wear mechanisms within hot stamping considering the influence of tool steel and hardness. *Wear* **2019**, *426*, 378–389. [CrossRef]
- Liu, H.; Sun, F.E.; Sun, H.E.; Liu, B.; Wang, Y.; Jin, X. Analysis of microstructure and mechanical properties of ultrafine grained low carbon steel. *J. Wuhan Univ. Technol. Mater. Sci. Ed.* **2016**, *31*, 1099–1104. [CrossRef]
- Cavusoglu, O.; Cavusoglu, O.; Yilmazoglu, A.G.; Üzel, U.; Aydin, H.; Güral, A. Microstructural features and mechanical properties of 22MnB5 hot stamping steel in different heat treatment conditions. *J. Mater. Res. Technol.* **2020**, *9*, 10901–10908. [CrossRef]
- Merklein, M.; Lechner, J.; Geiger, M. Characterisation of the Flow Properties of the Quenchenable Ultra High Strength Steel 22MnB5. *Ann. CIRP* **2006**, *55*, 229–232. [CrossRef]
- Gracia-Escosa, E.; García, I.; Damborenea, J.J.D.; Conde, A. Friction and wear behaviour of tool steels sliding against 22MnB5 steel. *J. Mater. Res. Technol.* **2017**, *6*, 241–250. [CrossRef]
- Huang, W.; Gu, H.; Liu, Q.; Si, T. Suppression of hydrogen-induced damage in 22MnB5 hot stamping steel by microalloying. *Mater. Chem. Phys.* **2020**, *256*, 123729. [CrossRef]
- Nassiraei, H.; Lotfollahi-Yaghin, M.A.; Neshaei, S.A.; Zhu, L. Structural behavior of tubular X-joints strengthened with collar plate under axially compressive load at elevated temperatures. *Mar. Struct.* **2018**, *61*, 46–61. [CrossRef]
- Maleki, E.; Unal, O.; Amanov, A. Novel experimental methods for the determination of the boundaries between conventional, severe and over shot peening processes. *Surf. Interfaces* **2018**, *13*, 233–254. [CrossRef]
- Maleki, E.; Unal, O.; Kashyzadeh, K.R. Effects of conventional, severe, over, and re-shot peening processes on the fatigue behavior of mild carbon steel. *Surf. Coat. Technol.* **2018**, *344*, 62–74. [CrossRef]
- Maleki, E.; Unal, O.; Kashyzadeh, K.R. Surface layer nanocrystallization of carbon steels subjected to severe shot peening: Analysis and optimization. *Mater. Charact.* **2019**, *157*, 109877. [CrossRef]
- Maleki, E.; Unal, O.; Reza Kashyzadeh, K. Fatigue behavior prediction and analysis of shot peened mild carbon steels. *Int. J. Fatigue* **2018**, *116*, 48–67. [CrossRef]
- Ganapathy, M.; Li, N.; Lin, J.; Bhattacharjee, D. A feasibility study on warm forming of an as-quenched 22MnB5 boron steel. *Int. J. Lightweight Mater. Manuf.* **2020**, *3*, 277–283. [CrossRef]
- Mu, Y.; Wang, B.; Zhou, J.; Kang, Y.; Li, X. Heating parameters optimization of hot stamping by partition heating for tailored properties. *ISIJ Int.* **2017**, *57*, 1442–1450. [CrossRef]
- Merklein, M.; Wieland, M.; Lechner, M.; Bruschi, S.; Ghiotti, A. Hot stamping of boron steel sheets with tailored properties: A review. *J. Mater. Process. Technol.* **2016**, *228*, 11–24. [CrossRef]
- Vrolijk, M.; Lorenz, D.; Porzner, H.; Holecek, M. Supporting lightweight design: Virtual Modeling of hot stamping with tailored properties and warm and hot formed aluminium. *Procedia Eng.* **2017**, *183*, 336–342. [CrossRef]

20. Mori, K.; Maeno, T.; Mongkolkaji, K. Tailored die quenching of steel parts having strength distribution using bypass resistance heating in hot stamping. *J. Mater. Process. Technol.* **2013**, *213*, 508–514. [[CrossRef](#)]
21. Mu, Y.; Wang, B.; Zhou, J.; Simonetto, E.; Ghiotti, A.; Bruschi, S. Laboratory trials and design of industrial application of hot stamping of 22MnB5 tailored components by partition heating. *Procedia Manuf.* **2018**, *15*, 1103–1110. [[CrossRef](#)]
22. Lin, L.; Li, B.-s.; Zhu, G.-m.; Kang, Y.-l.; Liu, R.-d. Effects of Nb on the microstructure and mechanical properties of 38MnB5 steel. *Int. J. Miner. Metall. Mater.* **2018**, *25*, 1181–1190. [[CrossRef](#)]
23. Liang, X.; Li, X.; Wang, D.; Lin, X.; Luo, P.; Tan, Z.; Song, Y.; Tian, Y.; Hou, J.; Jiang, C.; et al. Numerical and Experimental Study on Hot Forming by Partition Cooling of 38MnB5Nb. *Metals* **2022**, *12*, 839. [[CrossRef](#)]
24. da Costa Ximenes, D.A.; Moreira, L.P.; de Carvalho, J.E.R.; Leite, D.N.F.; Toledo, R.G.; da Silva Dias, F.M. Phase transformation temperatures and Fe enrichment of a 22MnB5 Zn-Fe coated steel under hot stamping conditions. *J. Mater. Res. Echnol.* **2020**, *9*, 629–635. [[CrossRef](#)]
25. Gao, G.; Feng, C.; Bai, B. Effects of Nb on the Microstructure and Mechanical Properties of Water-Quenched F_{GBA}/B_G Steels. *J. Mater. Eng. Perform.* **2012**, *21*, 345–352. [[CrossRef](#)]
26. Gao, B.; Tan, Z.; Luo, P.; Gao, G.; Zhang, M.; Misra, R.; Bai, B. Bainitic austempering incorporating quenching and partitioning for favorable tuning of microstructure and mechanical properties. *Steel Res. Int.* **2020**, *91*, 1900510. [[CrossRef](#)]
27. Zhu, L.; Gu, Z.; Xu, H.; Lv, Y.; Chao, J. Modeling of Microstructure Evolution in 22MnB5 Steel during Hot Stamping. *J. Iron Steel Res. Intl.* **2014**, *21*, 197–201. [[CrossRef](#)]

Disclaimer/Publisher’s Note: The statements, opinions and data contained in all publications are solely those of the individual author(s) and contributor(s) and not of MDPI and/or the editor(s). MDPI and/or the editor(s) disclaim responsibility for any injury to people or property resulting from any ideas, methods, instructions or products referred to in the content.